Essential Supplementary Information (ESI)

Self-derivation High-Mechanical-Strength Polymetallic Phosphides Microsheets Heterostructures for Industrial-scale High Current Density Water Splitting

Jing Jin[a], Feng Chen[a], Xinyu Hu[a], Jiashuai Zhang[a], Li Hou[a], Wenwei Lei[a], Faming Gao*[a,b]*

[a]Hebei Key Laboratory of Applied Chemistry, State Key Laboratory of Metastable Materials Science and Technology, Yanshan University, Qinhuangdao 066004, China.

[b]College of Chemical Engineering and Materials science, Tianjin University of Science and Technology, Tianjin 300457, China.

** Corresponding author. E-mail: holy@ysu.edu.cn; fmgao@ysu.edu.cn*

Experimental

Materials:

Hydrochloric acid (HCl), Anhydrous Ethanol (C_2H_5OH), Potassium Hydroxide (KOH), Ferric nitrate nonahydrate ($Fe(NO_3)_3$ $9H_2O$), Urea (CH_4N_2O), Sodium Hypophosphite (NaH_2PO_2), Commercial Platinum Carbon (Pt/C), Ruthenium Oxide (RuO_2) and Nafion (5 wt%). All reagents purchased from Aladdin Ltd. (Shanghai, China) were used as raw materials without further purification. Ni-Co foam (NCF, Ni : Co = 1 : 9) with a thickness of 1mm was purchased from Guangshengjia new material Co. Ltd. Further processing is required before use. The deionized water used in all experiments was purified by the Millipore system.

Preparation of Fe_X-CoNi(OH)/NCF Pre:

Typically, the Ni-Co foam was cut into a size of 0.5*0.5 cm^2, and was cleaned by ultrasonic cleaning with 1 M hydrochloric acid, and anhydrous ethanol for 20 min in order to remove the oxide and organic layer on the surface, then washed with deionized water and dried in a vacuum oven for several hours for the next step. The Fe_X-CoNi(OH)/NCF precursor was grown on the NCF using a simple hydrothermal method. In brief, 5 mmol urea and X mmol (X = 0, 0.1, 0.3, and 0.5) $Fe(NO_3)_3$ $9H_2O$ were evenly dissolved into 30 mL deionized water through magnetic stirring. The obtained solution and the cleaned NCF foam were transferred to a 50 mL Teflon-lined stainless steel reactor, which was heated at 150℃ for 12 hours. Subsequently, the reaction was completed, and it was naturally cooled down to room temperature. The

Fe_X-CoNi(OH)/NCF precursor was removed and rinsed repeatedly with deionized water to remove excess impurities, and dried at 60℃ in a vacuum oven.

Preparation of Fe_X-CoNiP/NCF:

The obtained Fe_X-CoNi(OH)/NCF precursor was phosphorylated by the pyrolysis of NaH_2PO_2 under the protection of nitrogen. The Fe_X-CoNi(OH)/NCF precursor and 0.4 g NaH_2PO_2 were located at the downstream and upstream side of the tube furnace, about 10 cm apart, respectively. The boats were placed in the middle of a tubular furnace, heated to 300℃ for 2 h with a rate of 5℃ per minute in N_2 atmosphere. The final sample was obtained after cooling, denoted as Fe_X-CoNiP/NCF.

Preparation of Pt/C and RuO_2 catalysts on NCF:

Pt/C powder (4 mg, 20 wt%), and carbon black (2 mg, Vulcan XC72) were dissolved in a solution containing 50 μL Nafion, and 950 μL water/ethanol (V: V=1:1), and the mixture was uniformly dispersed by ultrasound for 30 min. The paste was then evenly coated on both sides of the treated copper foam and dried in a vacuum drying oven at 60°C for 12 h to produce an electrode loaded with Pt/C catalyst, noted as Pt/C@NCF. The RuO_2@NCF electrode was prepared by the same procedure with RuO_2 powder (4 mg, 20 wt%).

Materials Characterization.

The phase structure of the samples was characterized with a powder X-ray diffractometer (XRD) (Cu Kα, λ = 1.5418 Å) at a scanning speed of 3° min^{-1} in the

range of 20-80°. The morphology of the samples were observed by field emission scanning electron microscopy (SEM, JEOL, JEM-2010) and transmission electron microscopy (TEM, JEOL, JEM-2010). The composition and distribution of the elements of the samples were analyzed by energy-dispersive X-ray spectroscopy (EDS) attached to the transmission electron microscopy. The SDC-350 contact Angle tester produced by Dongguan Shengding Precision Instrument. The chemical composition and surface electronic states of the samples were studied by X-ray photoelectron spectroscopy recorded on an ESCA-LAB MKII device with a monochromatic Al-K-α X-ray source. Meanwhile, Raman spectroscope (Horiba iHR550) was used for checking the frame structures of catalysts.

Electrochemical Measurements.

All samples were tested for their electrochemical performance using the Shanghai C&H CHI 760E instrument in a three-electrode setup. A standard three-electrode system comprised a reference electrode (Hg/HgO), counter electrode (graphite rod), and the prepared sample the prepared sample itself, serving as the working electrode (0.5*0.5 cm^2), respectively. The electrolyte was 1.0 M KOH solution for all tests, with the exception of the overall water splitting tests, this testing utilized a 6.0 M KOH electrolyte to simulate the electrolysis of water under industrial conditions. The linear scanning voltammetry (LSV) curves were performed at a sweep rate of 5 mV s^{-1}, and subsequently, the overpotential at different current densities (j) was calculated. For comparison, the NCF coated with 20 wt% Pt/C and RuO_2 with the

same mass loading rate as the $CoNiFe_XP$/NCF, served as the electrodes for the hydrogen evolution reaction (HER) and oxygen evolution reaction (OER), respectively. In order to reveal the intrinsic behavior of the catalysts, 85% IR compensation was employed to eliminate the effect of Ohmic resistance. It was converted to the reversible hydrogen electrode (RHE) according to the Nernst equation: E(RHE) = E(Hg/HgO) + 0.098 + 0.059 * pH. Unless explicitly specified, the potential values are referenced to the reversible hydrogen electrode (vs. RHE) in this work. The Tafel slope was determined from the LSV curve through plotting the potential against the logarithm of the current density. The bilayer capacitance (C_{dl}) of the samples was assessed by cyclic voltammetry (CV) measurements at different sweep rates within the non-Faraday range, in accordance with the electrochemically active surface area (ECSA). Specifically, the CV data was recorded from 0.276 to 0.326 V (vs RHE) for HER and from 0.926 to 0.976 V (vs RHE) for OER with different scanning rates ranging from 80 to 200 mV s^{-1}. The capacitive current is linearly related to the scan rate, corresponding to a slope twice as large as C_{dl}. The electrochemical impedance spectroscopy (EIS) was measured at different potentials across a frequency range spanning 0.01 Hz to 100 kHz. The long-term stability assessments were performed using chronoamperometry under constant current conditions. Faradic efficiency was determined by the drainage method during the HER and OER process.

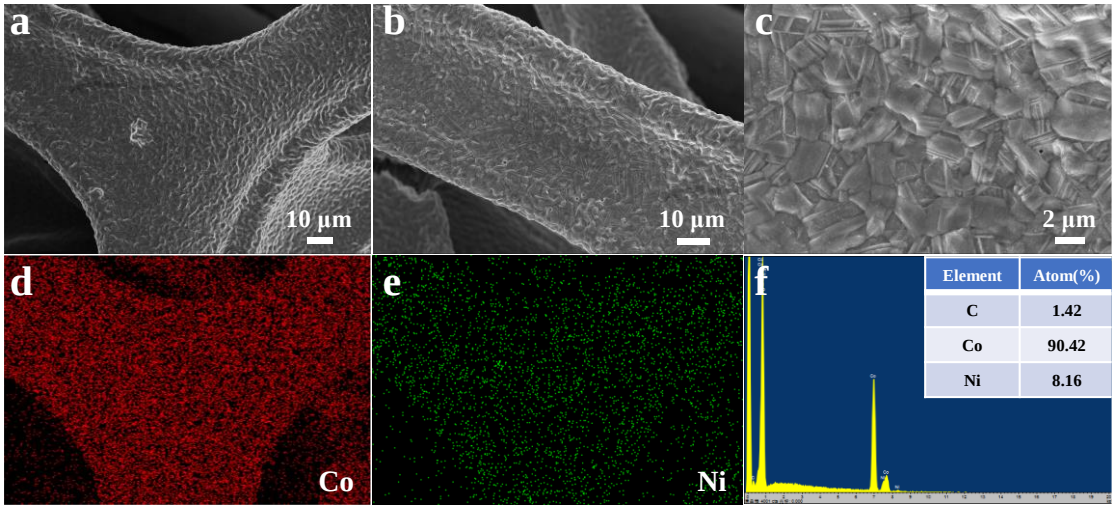

Fig. S1. SEM images (a-c) and EDX spectrum (d-f) of nickel-cobalt foam.

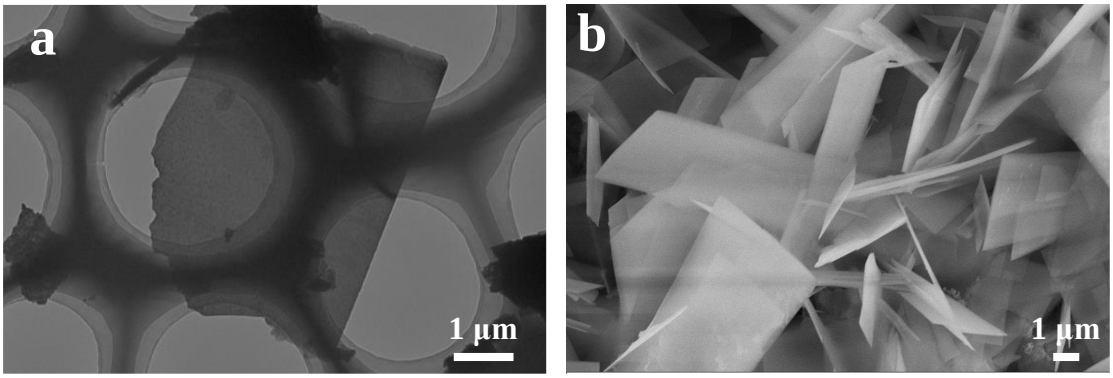

Fig. S2. (a) TEM and (b) SEM images of Fe-CN(OH)/NCF.

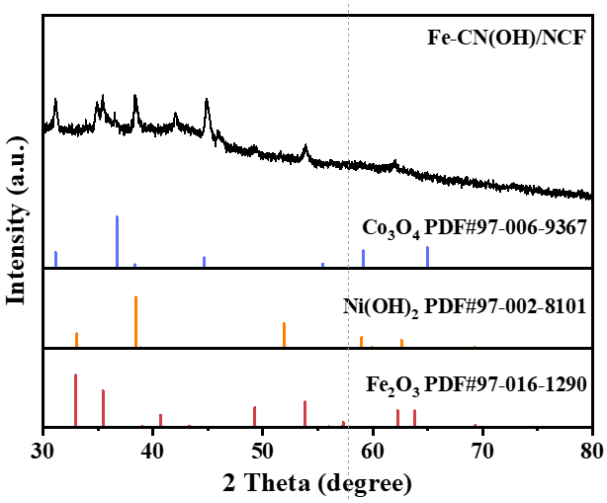

Fig. S3. The XRD pattern of Fe-CN(OH)/NCF.

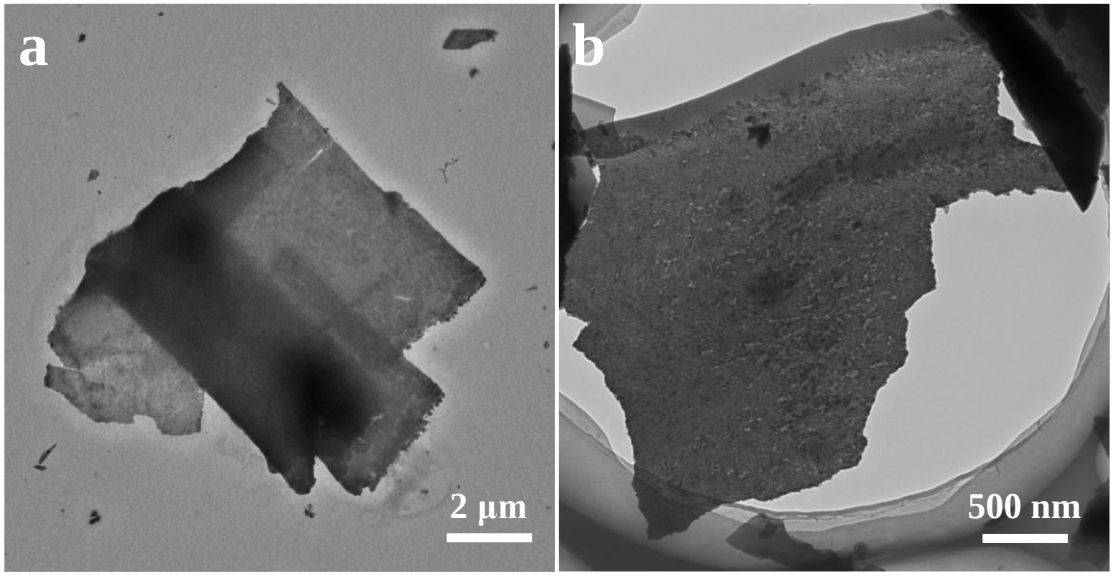

Fig. S4. (a) TEM images of Fe-CNP/NCF at different magnification.

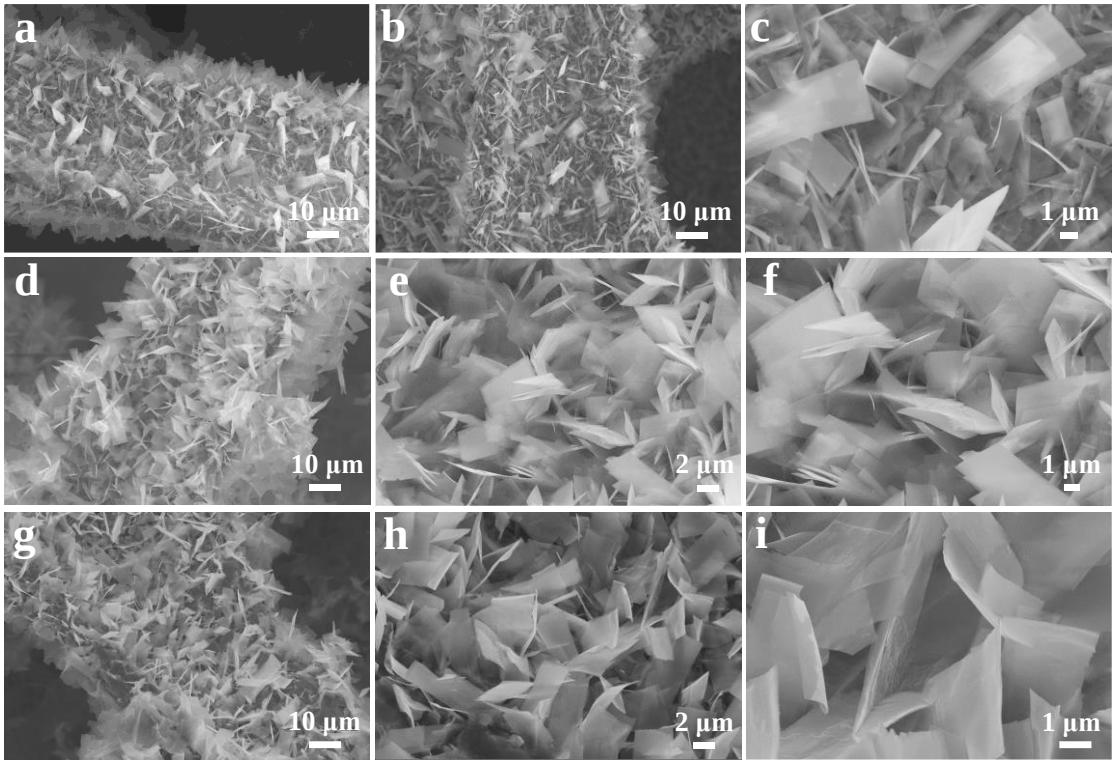

Fig. S5. SEM images of Fe_x-CNP/NCF at different magnification, (a-c) x=0, (d-f) x=0.1, (g-i) x=0.5.

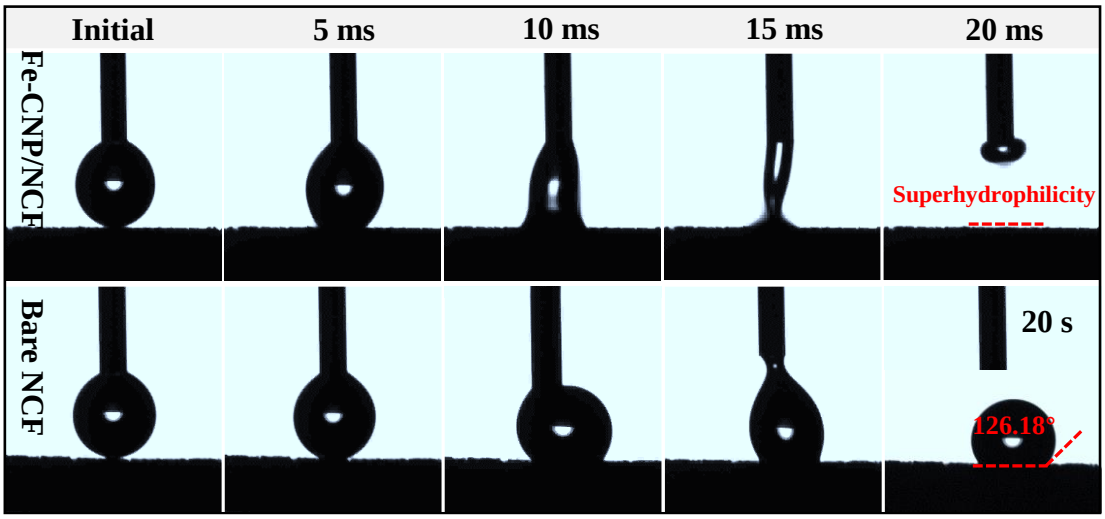

Fig. S6. The contact angel test of Fe-CNP/NCF and Bare NCF.

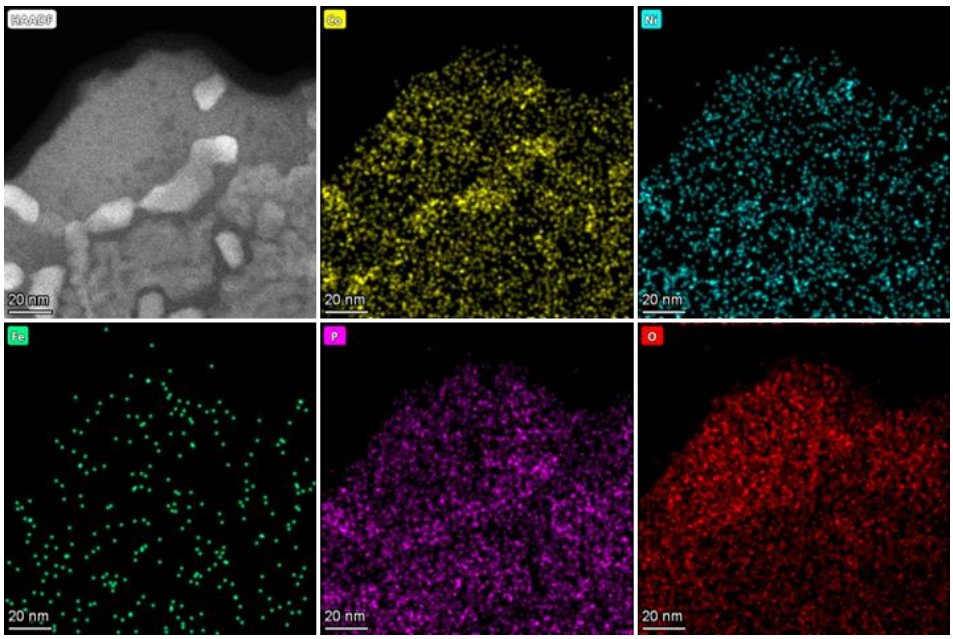

Fig. S7. The STEM images and EDX elemental mapping images of Co, Ni, Fe, P and O for the Fe-CNP/NCF sample.

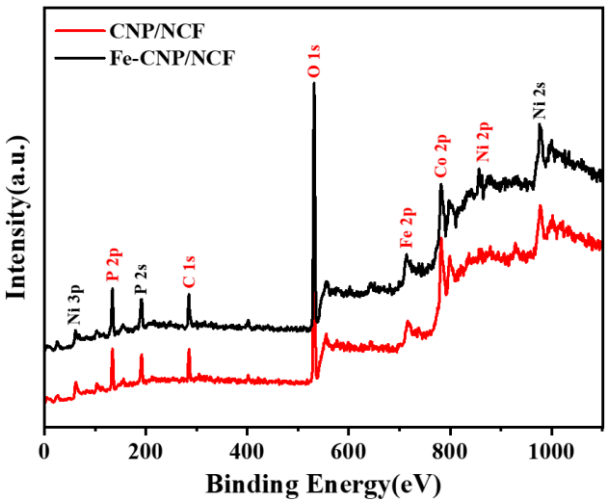

Fig. S8. XPS spectra in the regions of survey spectra for CNP/NCF and Fe-CNP/NCF.

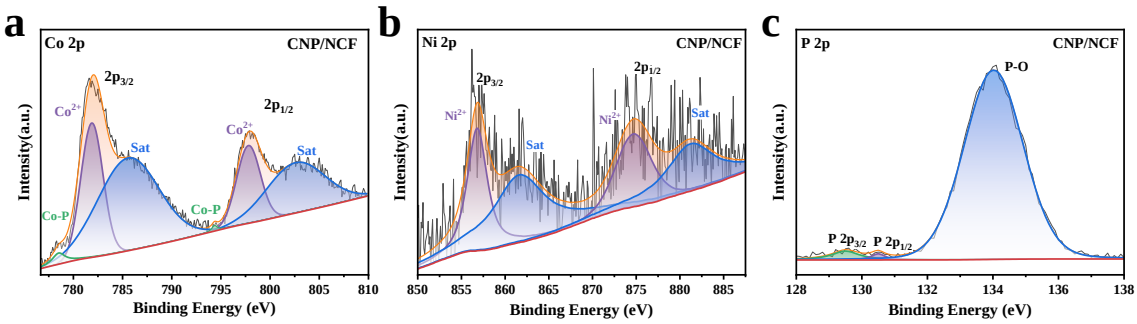

Fig. S9. XPS spectra of CNP/NCF catalyst samples: (a) Co 2p, (b) Ni 2p and (c) P 2p.

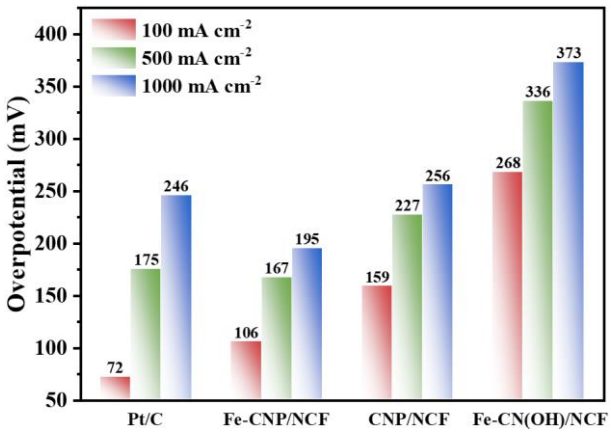

Fig. S10. Overpotential histogram of different samples at the current density of 100, 500 and 1000 mA cm^{-2} for HER.

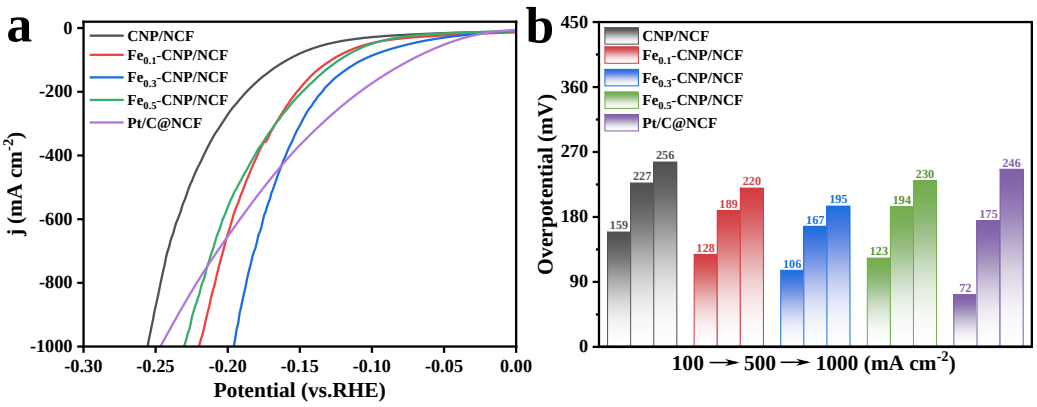

Fig. S11. HER catalytic activity of Fe_X-CNP/NCF (X=0, 0.1, 0.3 and 0.5) (a) Polarization curve (LSV) in 1.0 M KOH solution; (b) Overpotential histogram at a current density of 100, 500 and 1000 mA cm^{-2}.

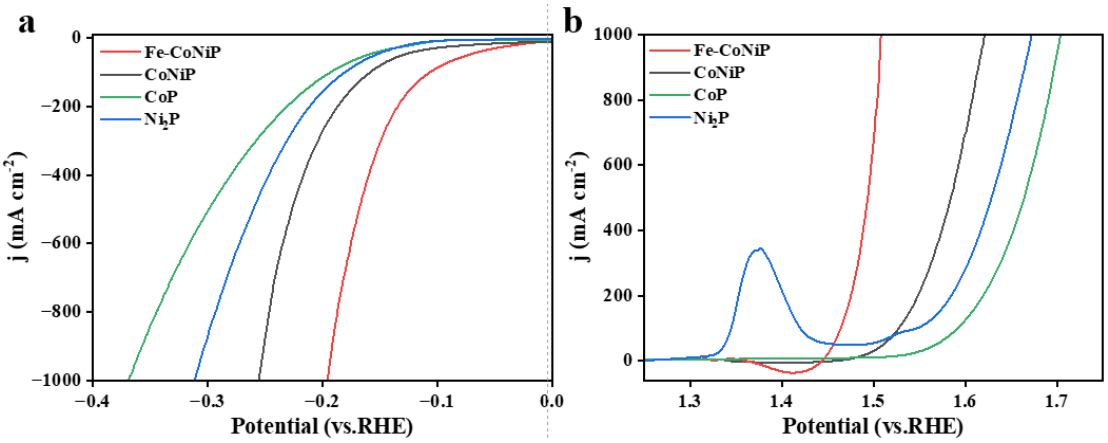

Fig. S12. Polarization curve (LSV) in 1.0 M KOH solution of different samples (a) HER; (b) OER.

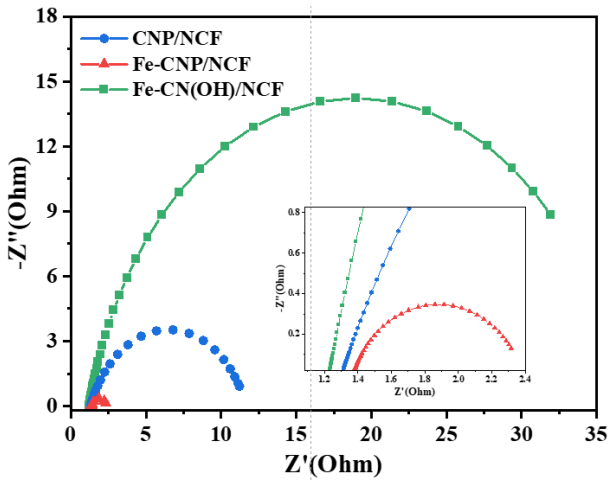

Fig. S13. EIS plots of different samples for HER.

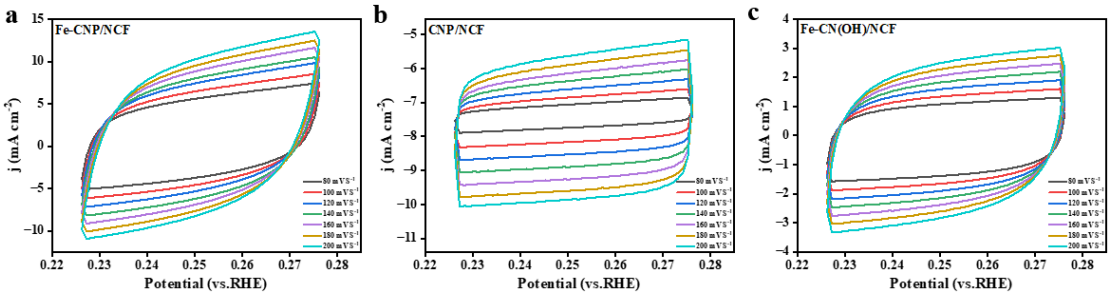

Fig. S14. CV curves of different samples for HER at scan rates from 80 to 200 mV s^{-1}.

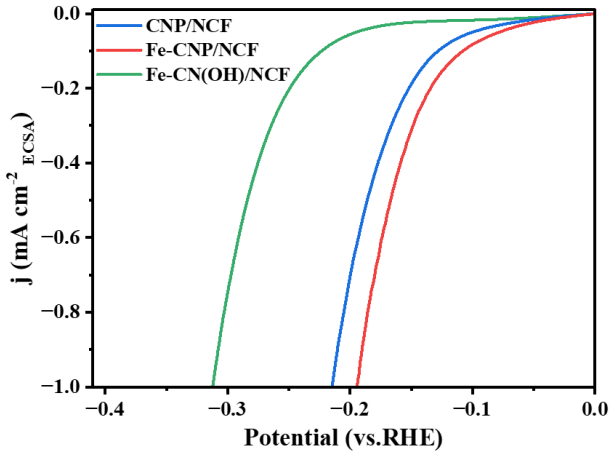

Fig. S15. The LSV curves of different samples normalized to the ECSA.

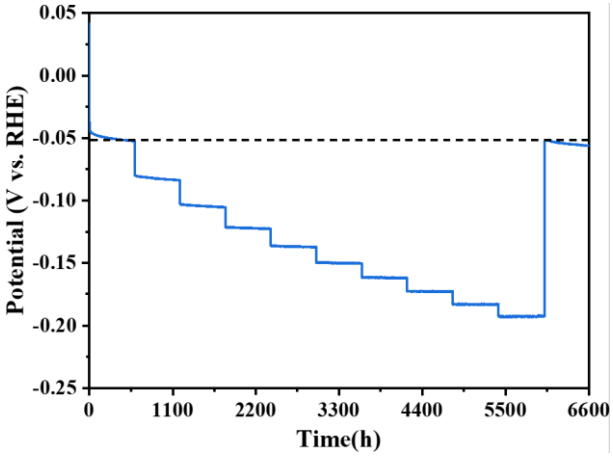

Fig. S16. Multi-potential curve of Fe-CNP/NCF for HER.

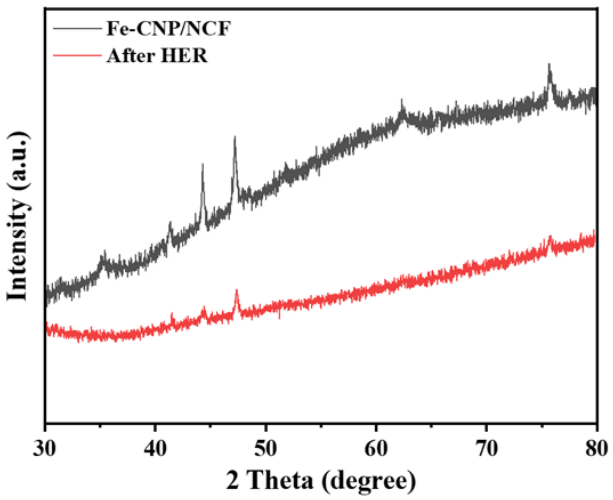

Fig. S17. XRD pattern of Fe-CNP/NCF after stability test for HER.

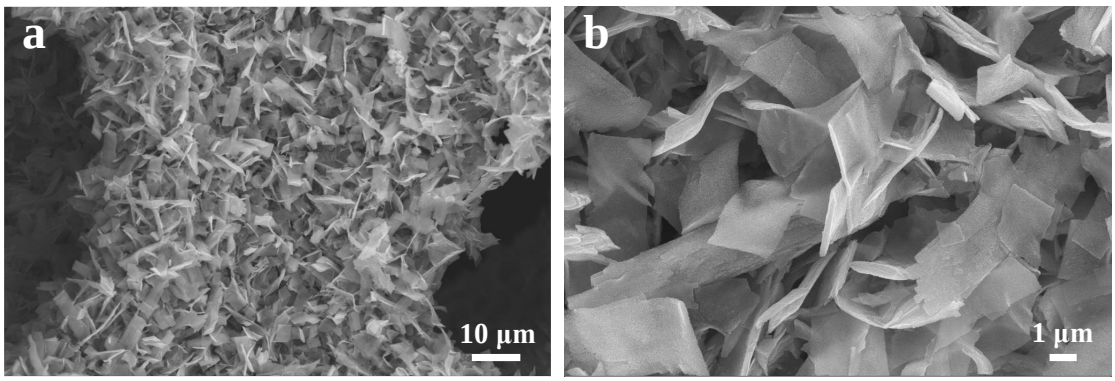

Fig. S18. SEM images of Fe-CNP/NCF after stability test for HER.

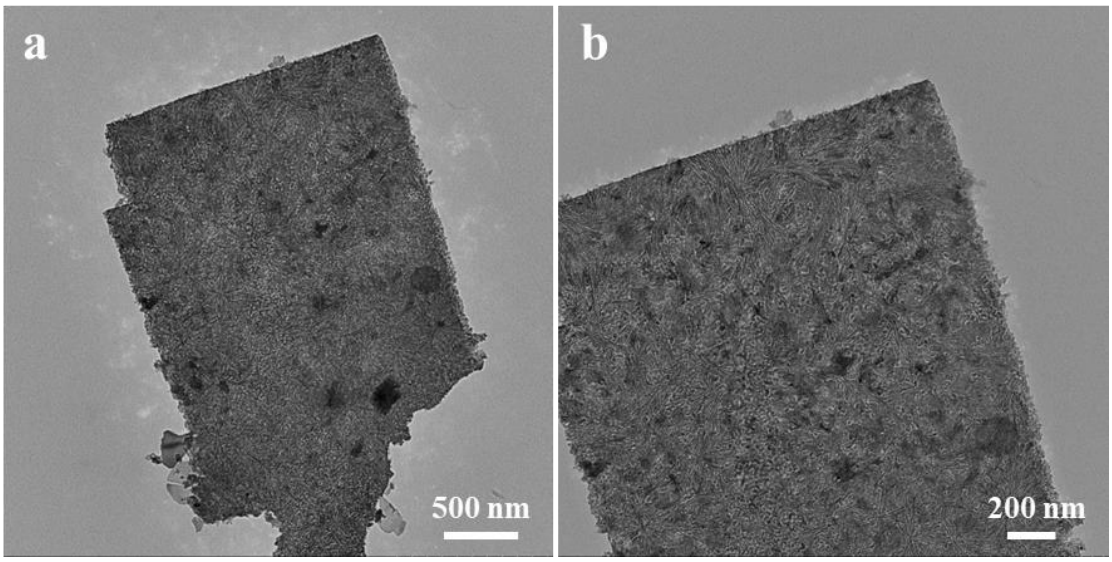

Fig. S19. TEM images of Fe-CNP/NCF after stability test for HER.

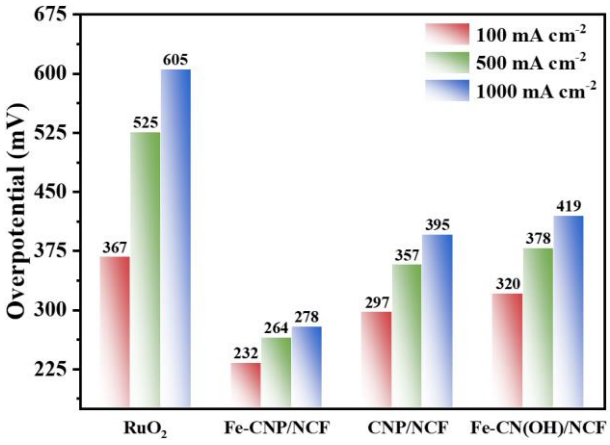

Fig. S20. Overpotential histogram of different samples at the current density of 100, 500 and 1000 mA cm^{-2} for OER.

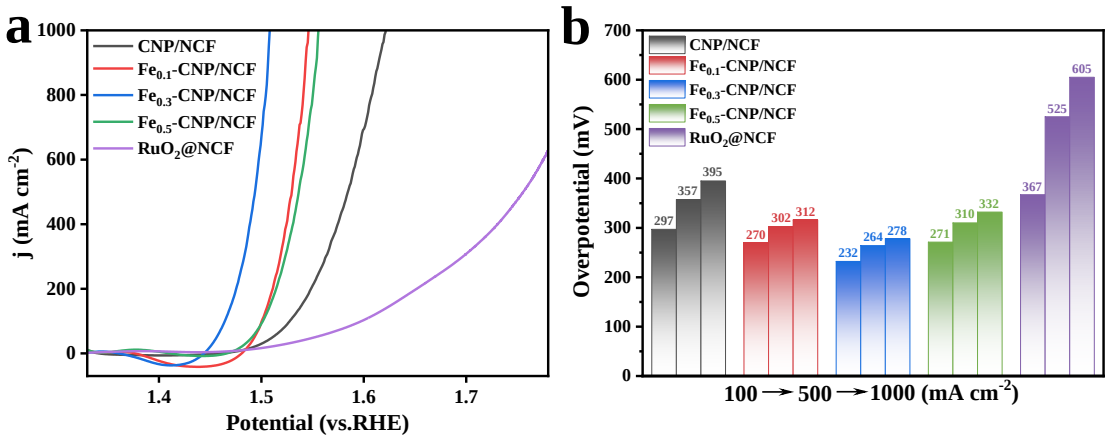

Fig. S21. OER catalytic activity of Fe_X-CNP/NCF (X=0, 0.1, 0.3 and 0.5) (a) Polarization curve (LSV) in 1.0 M KOH solution; (b) Overpotential histogram at a current density of 100, 500 and 1000 mA cm^{-2}.

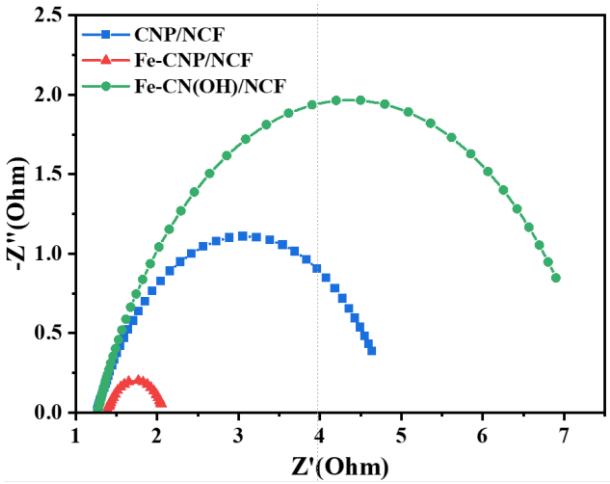

Fig. S22. EIS plots of different samples for OER.

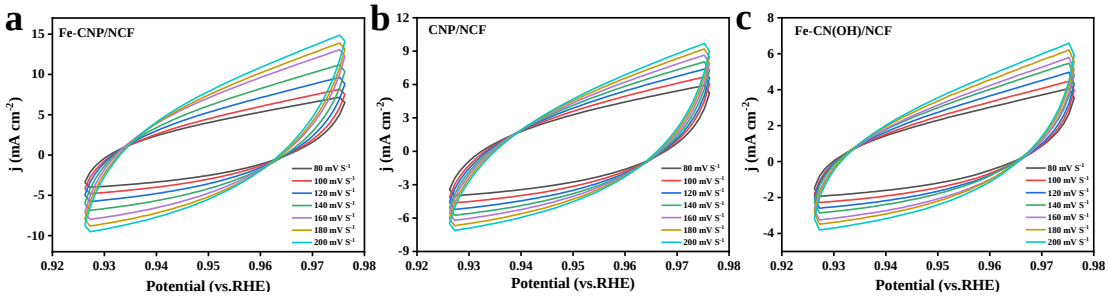

Fig. S23. CV curves of different samples for OER at scan rates from 80 to 200 mV s^{-1}.

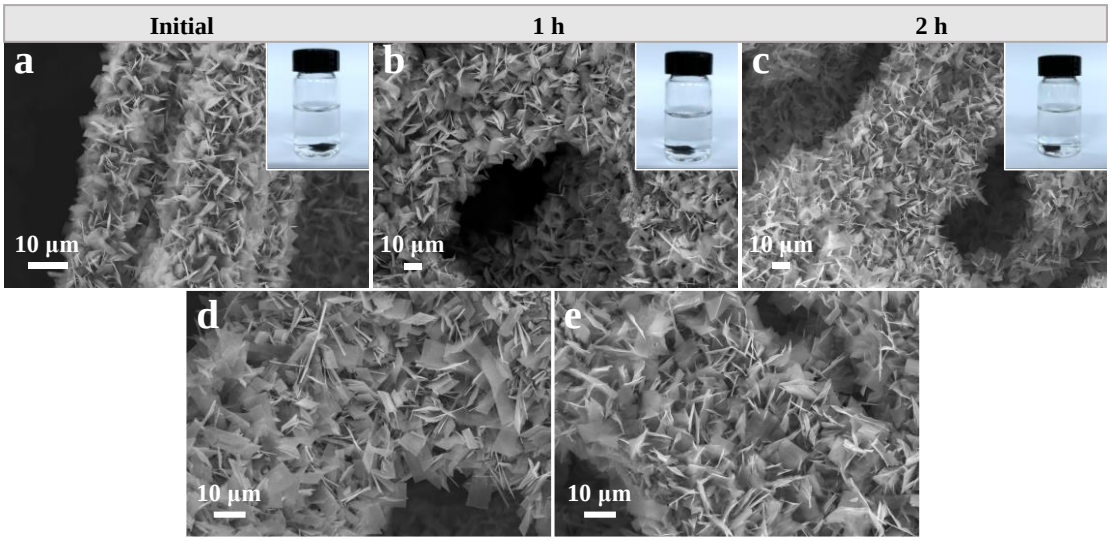

Fig. S24. SEM images of Fe-CNP/NCF after the accelerated mechanical strength test (a-c) sonicated; (d-e) ball milling.

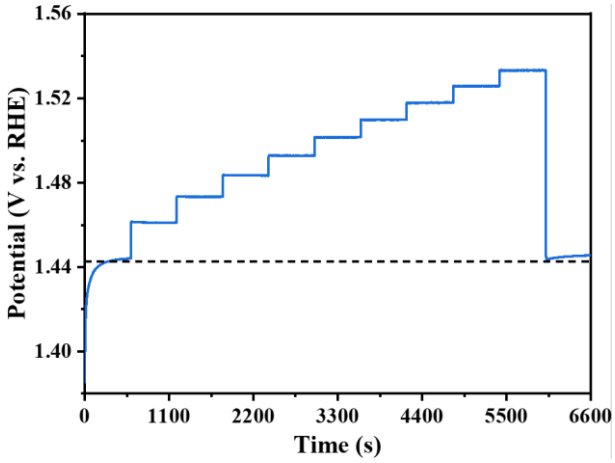

Fig. S25. Multi-potential curve of Fe-CNP/NCF for OER.

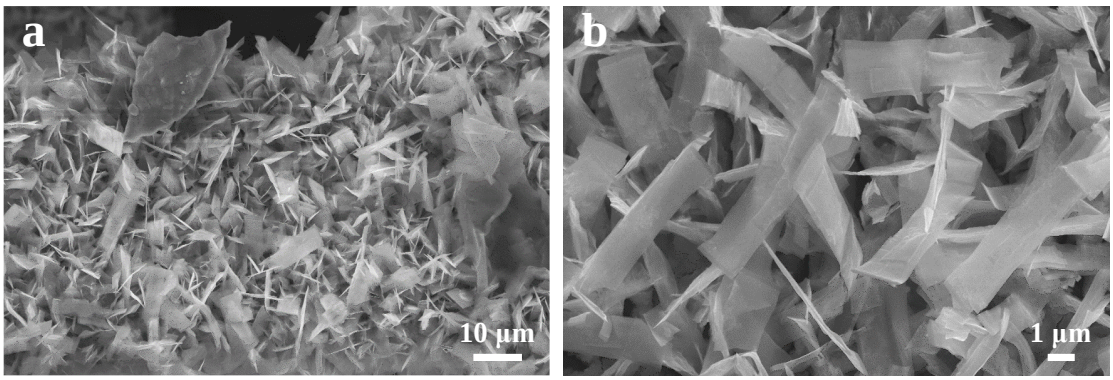

Fig. S26. SEM images of Fe-CNP/NCF after stability test for OER.

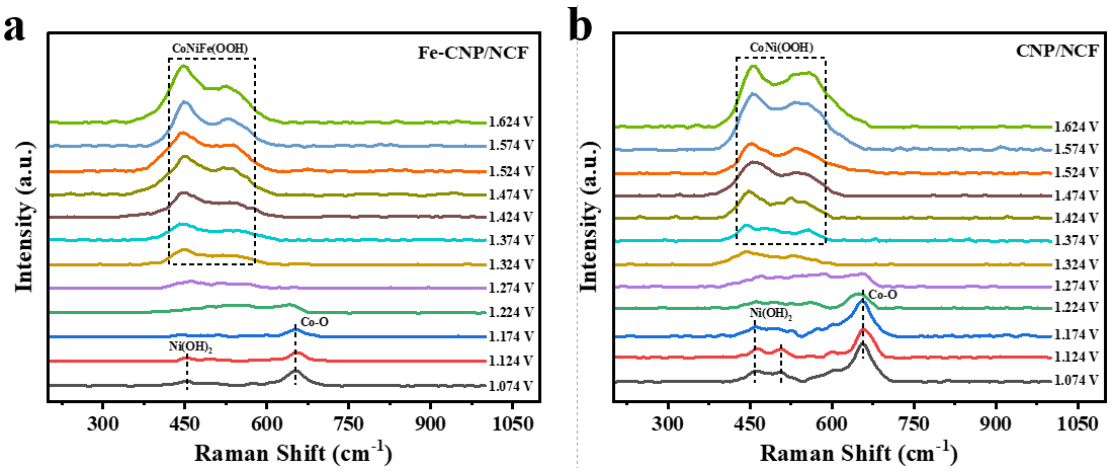

Fig. S27. In situ Raman plot of (a) Fe-CNP/NCF; (b) CNP/NCF.

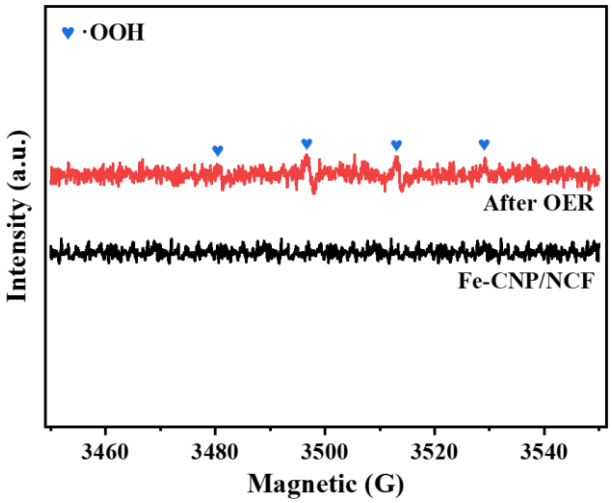

Fig. S28. EPR spectra of Fe-CNP/NCF before and after OER.

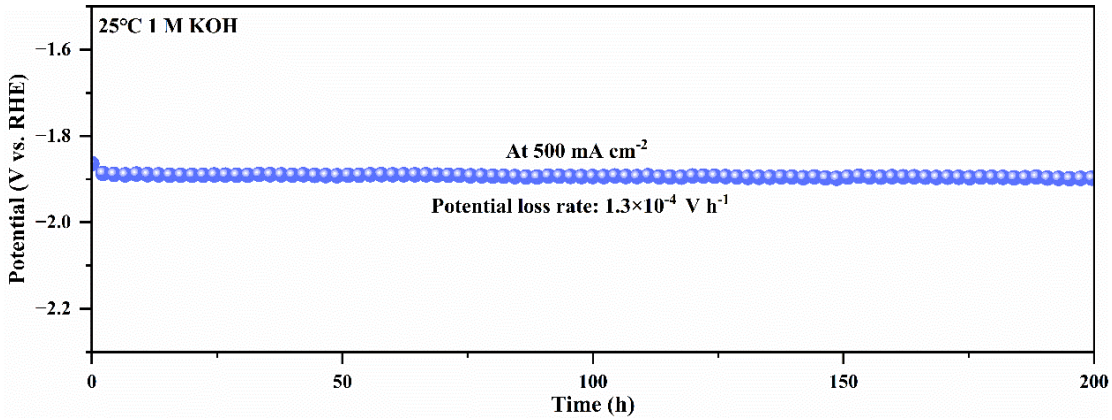

Fig. S29. Chronopotentiometry curve of Fe-CNP/NCF || Fe-CNP/NCF for overall

water splitting at 25℃, 1.0 M KOH electrolyte.

Electrocatalysts	η_{100}(mV)	η_{500}(mV)	Stability
Fe-CNP/NCF	106	167	150 h@500 mA cm^{-2}
$Co_2P/Ni_{12}P_5/NF$[1]	109	173	100 h@500 mA cm^{-2}
Cu-FeOOH/Fe_3O_4[2]	129	285	100 h@120 mV
CeO_2-NiCoP[3]	137	202	18 h@500 mA cm^{-2}
$M_xO@M_xP/PNCF$[4]	145	256	100 h@10 mA cm^{-2}
$NCF_{0.5}P$@CNT/CW[5]	226	269	120 h@50 mA cm^{-2}
Ni_2P-Fe_2P/NF[6]	225	298	24 h@100, 500 mA cm^{-2}
Mn-doped Ni_2P/Fe_2P[7]	268	365	100 h@500 mA cm^{-2}

Table S1. Comparison of HER catalysts performance between Fe-CNP/NCF and recently catalysts in 1 M KOH eleatrolyte.

Electrocatalysts	η_{100}(mV)	η_{500}(mV)	Stability
Fe-CNP/NCF	232	264	150 h@500 mA cm^{-2}
CoFe-Ni_2P[8]	235	277	130 h@100, 500 mA cm^{-2}
Mn-doped Ni_2P/Fe_2P[7]	254	304	100 h@500 mA cm^{-2}
$Fe_2P/Ni_{12}P_5$/NF[1]	256	305	100 h@500 mA cm^{-2}
Mo_2S_3@$NiMo_3S_4$[9]	256	345	24 h@100, 500 mA cm^{-2}
$(Fe,Ni)_2P$@Ni_2P[10]	268	307	65 h@1000 mA cm^{-2}
NiCoP/NF[11]	299	330	25 h@500 m A cm^{-2}
$NiCo_{(nf)}$-P[12]	315	378	30 h@100, 500, 1000 mA cm^{-2}

Table S2. Comparison of OER catalysts performance between Fe-CNP/NCF and recently catalysts in 1 M KOH eleatrolyte.

Electrocatalysts	Voltage$_{100}$ (V)	Voltage$_{500}$ (V)	Stability
Fe-CNP/NCF	1.57	1.67	200 h@500 mA cm^{-2}
CeO_2-NiCoP[3]	1.65	1.82	60 h@100, 200, 500 mA cm^{-2}
Ni_2P-Fe_2P[6]	1.68	1.86	48 h@100 mA cm^{-2}
P-MoS_2@CoP[13]	1.68	1.94	40 h@500 mA cm^{-2}
$(Fe,Ni)_2P$@Ni_2P[10]	1.70	1.83	120 h@200 mA cm^{-2}
CoFe-Ni_2P[8]	1.73	1.84	100 h@500 mA cm^{-2}
$NiCo_{(nf)}$-P[12]	1.74	1.86	30 h@100, 500,1000 mA cm^{-2}
Co_2P/Ni_xP_y@NF[14]	1.74	1.95	120 h@100, 200, 500 m A cm^{-2}
Mn-doped Ni_2P/Fe_2P[7]	1.8	1.99	100 h@10, 100, 500 mA cm^{-2}

Table S3. Comparison of overall water splitting performance between Fe-CNP/NCF and recently catalysts in 1 M KOH eleatrolyte at room temperature.

Reference

1. L. Guo, X. Liu, Z. He, Z. Chen, Z. Zhang, L. Pan, Z.-F. Huang, X. Zhang, Y. Fang and J.-J. Zou, Self-Supported Bimetallic Phosphide Heterojunction-Integrated Electrode Promoting High-Performance Alkaline Anion-Exchange Membrane Water Electrolysis, *ACS Sustainable Chem. Eng.*, 2022, **10**, 9956-9968.
2. C. Yang, W. Zhong, K. Shen, Q. Zhang, R. Zhao, H. Xiang, J. Wu, X. Li and N. Yang, Electrochemically Reconstructed Cu-FeOOH/Fe_3O_4 Catalyst for Efficient Hydrogen Evolution in Alkaline Media, *Adv. Energy Mater.*, 2022, **12**, 2200077.
3. X. Guo, M. Li, L. Qiu, F. Tian, L. He, S. Geng, Y. Liu, Y. Song, W. Yang and Y. Yu, Engineering electron redistribution of bimetallic phosphates with CeO_2 enables high-performance overall water splitting, *Chem. Eng. J.*, 2023, **453**, 139796.
4. Q. Zhang, W. Chen, G. Chen, J. Huang, B. Ouyang, D. Chen, E. Kan, T. Lan, C. Li, H.-S. Choi and K. K. Ostrikov, Trimetallic Octahedral Ni–Co–W Phosphoxide Sprouted from Plasma-Defect-Engineered Ni–Co Support for Ultrahigh-Performance Electrocatalytic Hydrogen Evolution, *ACS Sustainable Chem. Eng.*, 2021, **9**, 7454-7465.
5. C. Tian, S. Tian, S. Luo, L. Li, Y. Wu, Y. Qing and S. Yang, Rational Manipulation of Active CNT Encapsulated Fe Doped NiCoP Nanoparticles In Situ Grown in Hierarchically Carbonized Wood for High-Current-Density Water Splitting, *Small*, 2024, **20**, 2306970.
6. L. Wu, L. Yu, F. Zhang, B. McElhenny, D. Luo, A. Karim, S. Chen and Z. Ren, Heterogeneous Bimetallic Phosphide Ni_2P-Fe_2P as an Efficient Bifunctional Catalyst for Water/Seawater Splitting, *Adv. Funct. Mater.*, 2021, **31**, 2006484.
7. Y. Luo, P. Wang, G. Zhang, S. Wu, Z. Chen, H. Ranganathan, S. Sun and Z. Shi, Mn-doped nickel–iron phosphide heterointerface nanoflowers for efficient alkaline freshwater/seawater splitting at high current densities, *Chem. Eng. J.*, 2023, **454**, 140061.
8. C. Huang, Q. Zhou, L. Yu, D. Duan, T. Cao, S. Qiu, Z. Wang, J. Guo, Y. Xie, L. Li and Y. Yu, Functional Bimetal Co-Modification for Boosting Large-Current-Density Seawater Electrolysis by Inhibiting Adsorption of Chloride Ions, *Adv. Energy Mater.*, 2023, **13**, 2301475.
9. T. Wu, S. Xu, Z. Zhang, M. Luo, R. Wang, Y. Tang, J. Wang and F. Huang, Bimetal Modulation Stabilizing a Metallic Heterostructure for Efficient Overall Water Splitting at Large Current Density, *Adv. Sci.*, 2022, **9**, 2202750.
10. Y. Li, X. Yu, J. Gao and Y. Ma, Structural and electronic modulation of $(Fe,Ni)_2P$@Ni_2P heterostructure for efficient overall water splitting at high current density, *Chem. Eng. J.*, 2023, **470**, 144373.
11. L. Li, W. Zou, Q. Ye, Q. Li, Q. Feng, J. Wei, X. Xu and F. Wang, Quasi-parallel nickel cobalt phosphide nanosheet arrays as highly efficient electrocatalyst for hydrogen evolution and overall water splitting at large current densities, *J. of Power Sources*, 2021, **516**, 230657.
12. Z. Xu, C.-L. Yeh, J.-L. Chen, J. T. Lin, K.-C. Ho and R. Y.-Y. Lin, Metal–Organic Framework-Derived 2D NiCoP Nanoflakes from Layered Double Hydroxide Nanosheets for Efficient Electrocatalytic Water Splitting at High Current Densities, *ACS Sustainable Chem. Eng.*, 2022, **10**, 11577-11586.
13. Y. Hu, H. Yu, L. Qi, J. Dong, P. Yan, T. Taylor Isimjan and X. Yang, Interface Engineering of Needle-Like P-Doped MoS_2/CoP Arrays as Highly Active and Durable Bifunctional Electrocatalyst for Overall Water Splitting, *ChemSusChem*, 2021, **14**, 1565-1573.
14. H. Liu, Y. Zhang, R. Ge, J. M. Cairney, R. Zheng, A. Khan, S. Li, B. Liu, L. Dai and W. Li,

Tailoring the electronic structure of Ni_5P_4/Ni_2P catalyst by Co_2P for efficient overall water electrolysis, *Applied Energy*, 2023, **349**, 121582.